nature geoscience

SUPPLEMENTARY INFORMATION

DOI: 10.1038/NGEO2563

Divergent trajectories of Antarctic surface melt under two twenty-first-century climate scenarios

Luke D. Trusel[1,2*], Karen E. Frey[2], Sarah B. Das[1], Kristopher B. Karnauskas[1], Peter Kuipers Munneke[3,4], Erik van Meijgaard[5], Michiel R. van den Broeke[3]

1 Department of Geology and Geophysics, Woods Hole Oceanographic Institution, Woods Hole, MA, 02543, USA
2 Graduate School of Geography, Clark University, Worcester, MA, 01610, USA
3 Institute for Marine and Atmospheric Research, Utrecht University, 3508 TA Utrecht, Netherlands
4 Swansea University, Department of Geography, Swansea, SA2 8PP, United Kingdom
5 Royal Netherlands Meteorological Institute, 3730 AE De Bilt, Netherlands
* Email: ltrusel@whoi.edu

Contains:

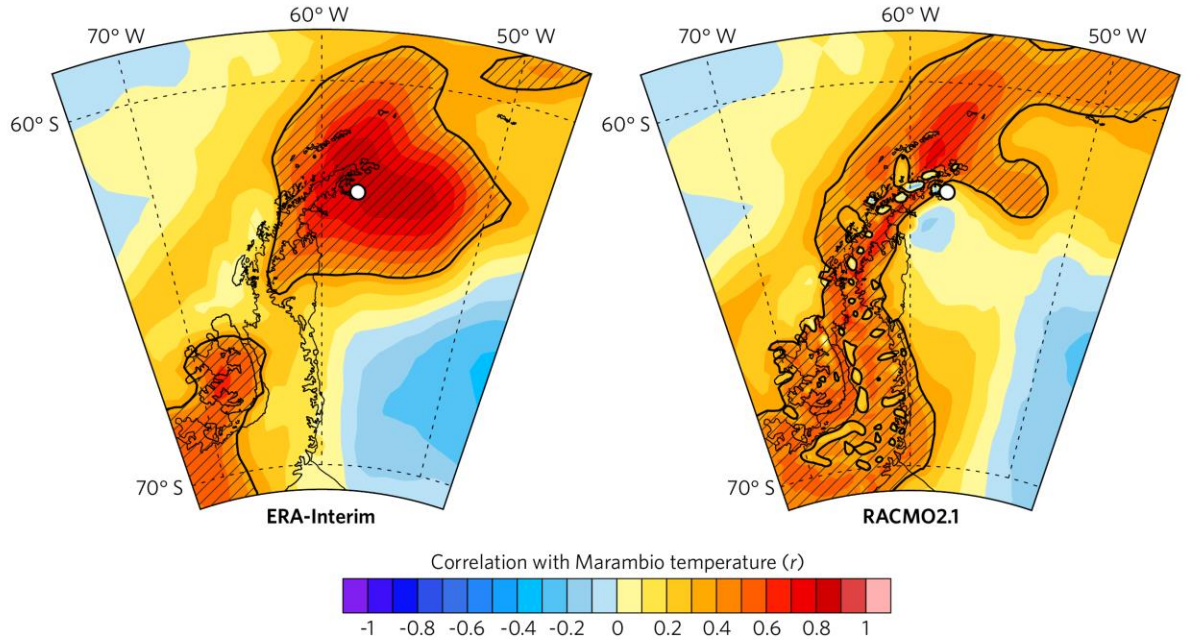

Supplementary Figure 1.
Spatial correlation coefficients (r) between observed DJF temperatures at Base Marambio[1] (location indicated by white dots) and DJF T_{2m} from ERA-Interim and RACMO over 1981–2009 (the time period of overlap with continuous observations). Areas of significant ($p \leq 0.05$) correlation indicated by hatching. Observed temperatures at Marambio broadly correlate with reanalyzed and modeled temperatures, particularly across the northeast Antarctic Peninsula and its ice shelves. As such, observed interannual summer temperature variability at Marambio can be interpreted as representative of broader Antarctic Peninsula conditions.

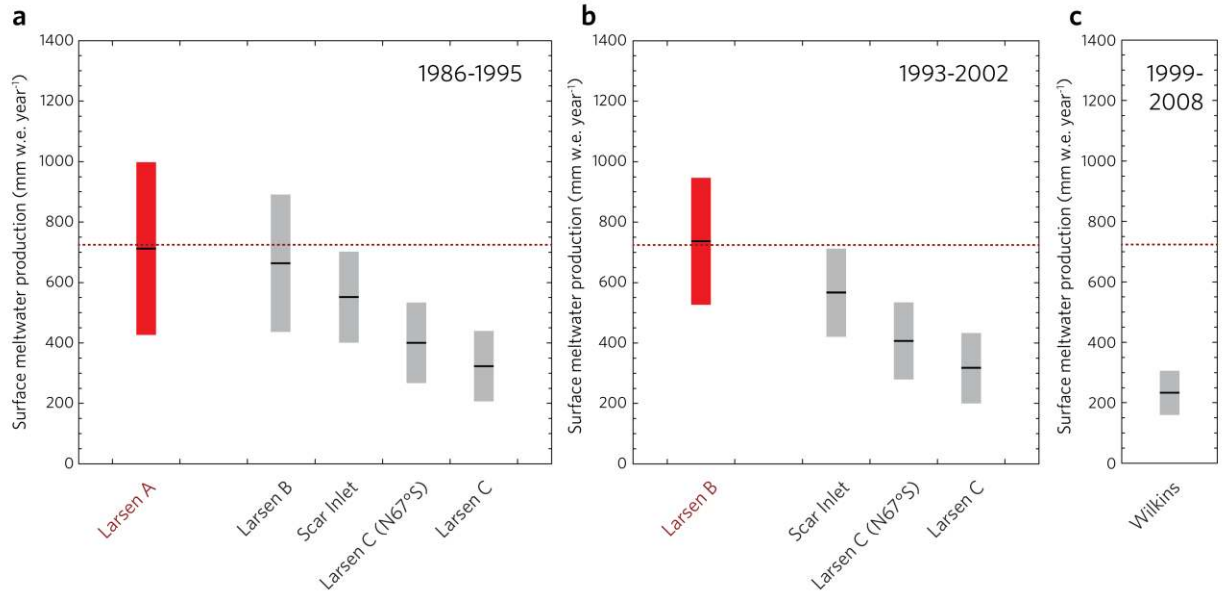

Supplementary Figure 2.
Mean melting conditions (± 1 temporal standard deviation) on Antarctic Peninsula ice shelves over the decades preceding the abrupt collapses of Larsen A (**a**, 1986–1995) and Larsen B (**b**, 1993–2002), and the more gradual breakup of Wilkins (**c,** 1999–2008). Melt data were averaged from two simulations of RACMO2 forced by ERA-Interim (27 and 48-km resolution), with the exception of Larsen A which was only resolved at 27-km resolution (Supplementary Table 1). Horizontal red dotted lines show the average pre-collapse melt of Larsen A and B (725 mm w.e. year^{-1}; as in Fig. 3b). Mean melt levels on northeast Antarctic Peninsula ice shelves that have remained intact (i.e., Scar Inlet, the high melt region of Larsen C north of 67°S, and Larsen C as a whole), experienced significantly ($p \leq 0.05$; two-tailed *t*-test) less melt than Larsen A and Larsen B. Whereas melt on the portion of Larsen B that collapsed in 2002 was not significantly different than Larsen A over 1986–1995 (**a**), its collapse followed rapid regional warming and coincided with extreme melt in 2002 (e.g., Fig. 2a). These results further demonstrate the linkage between locally high ice shelf melting and collapse events, while also supporting previous studies that have identified strong surface melt and hydrofracture as a leading mechanism in the abrupt collapses of Larsen A and B[2–4]. As an additional test of pre-breakup melt levels, we examined RACMO2-simulated melt on Wilkins Ice Shelf of the southwestern Antarctic Peninsula (**c**). This ice shelf has recently experienced more gradual retreat relative to Larsen A and B, with several breakup events occurring in summer, autumn, and winter of 2008 (for example, ref. 5). We find that in the decade preceding the 2008 Wilkins retreat, melt was significantly lower than that occurring on Larsen A and B before their abrupt collapses. This result supports work suggesting that surface melt played a more limited role in the breakup of Wilkins[6,7]. Nonetheless, others suggest the May 2008 breakup event may still have been in part related to surface melt-induced hydrofracture[5], underscoring the underlying complexity of ice shelf stability and response to external forcing.

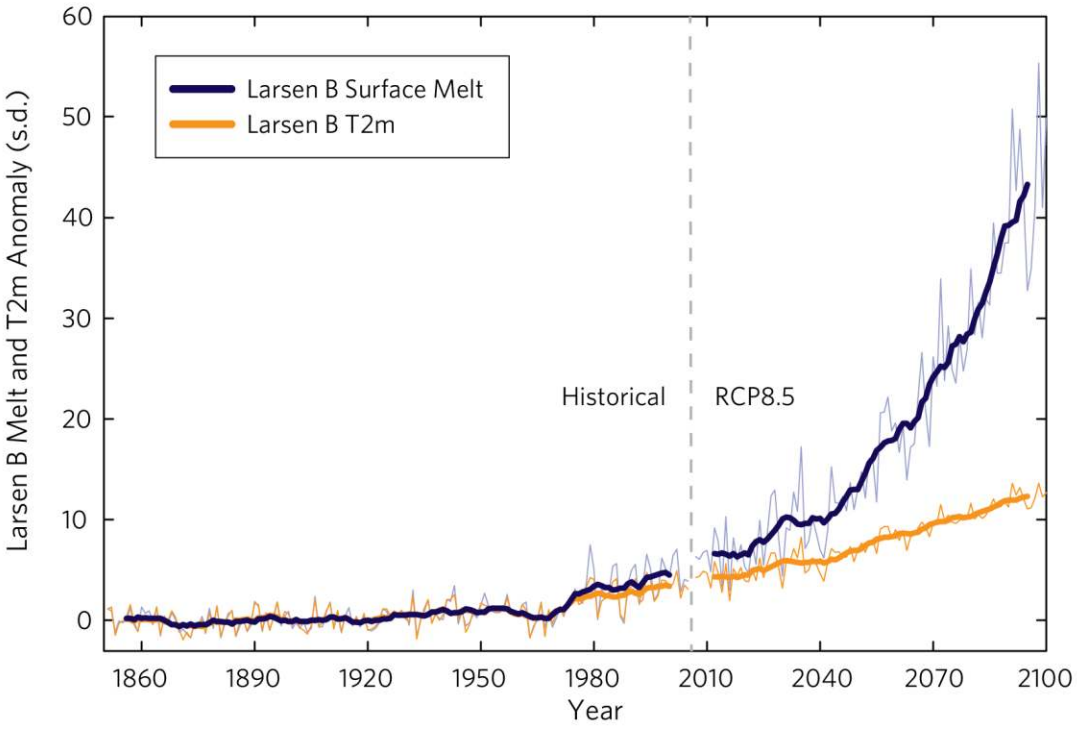

Supplementary Figure 3.
Anomalies in melt and temperature (with respect to 1851–1900) across Larsen B ice shelf. Anomalies from the GCM Ensemble Historical simulations (1851–2005) are shown as in Fig. 2c, whereas anomalies in the RCP8.5 scenario (2007–2100) are derived from the remaining portion of Larsen B ice shelf in Scar Inlet. Anomalies in melt far exceed anomalies in temperature owing to melt-temperature nonlinearity (see Fig. 1a).

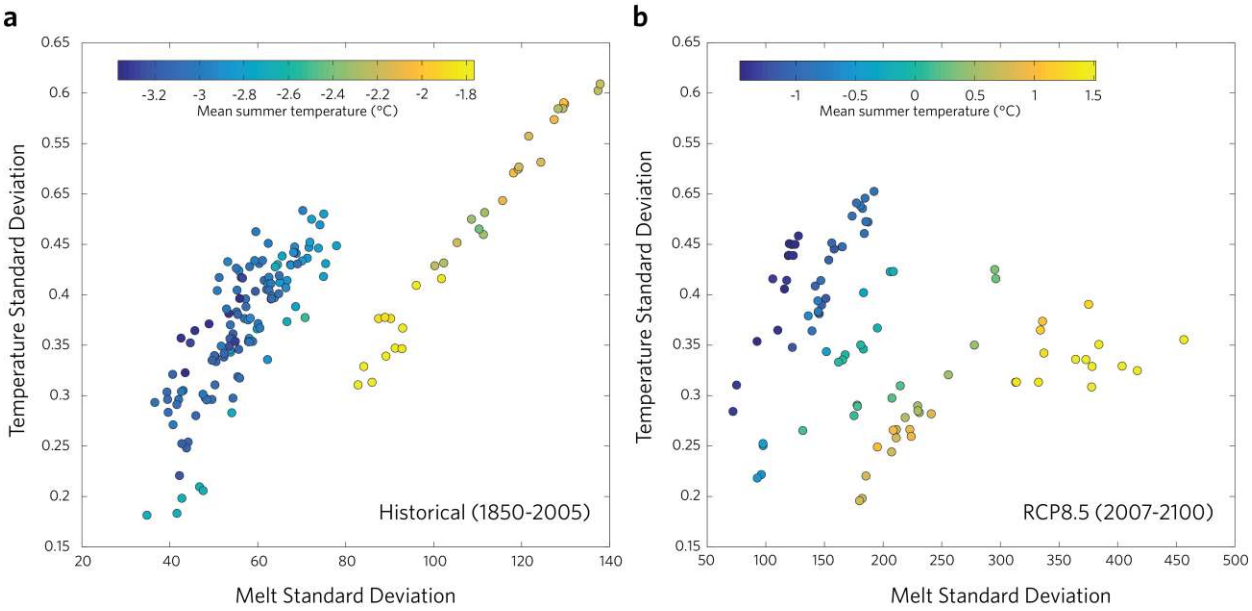

Supplementary Figure 4.
Plots of the 11-year moving temporal standard deviation of temperature and melt on Larsen B from Historical simulations (**a**) and RCP8.5 (**b**). Points are colored by mean summer temperature. (**a**) Abrupt warming occurring circa 1970 (Fig. 2b) resulted in a shift to higher interannual melt variability owing to the nonlinearity of melt in response to changing summer air temperature (Fig. 1a). (**b**) More gradual shifts toward higher interannual melt variability are simulated under a progressive RCP8.5 warming. Note unique x-axes.

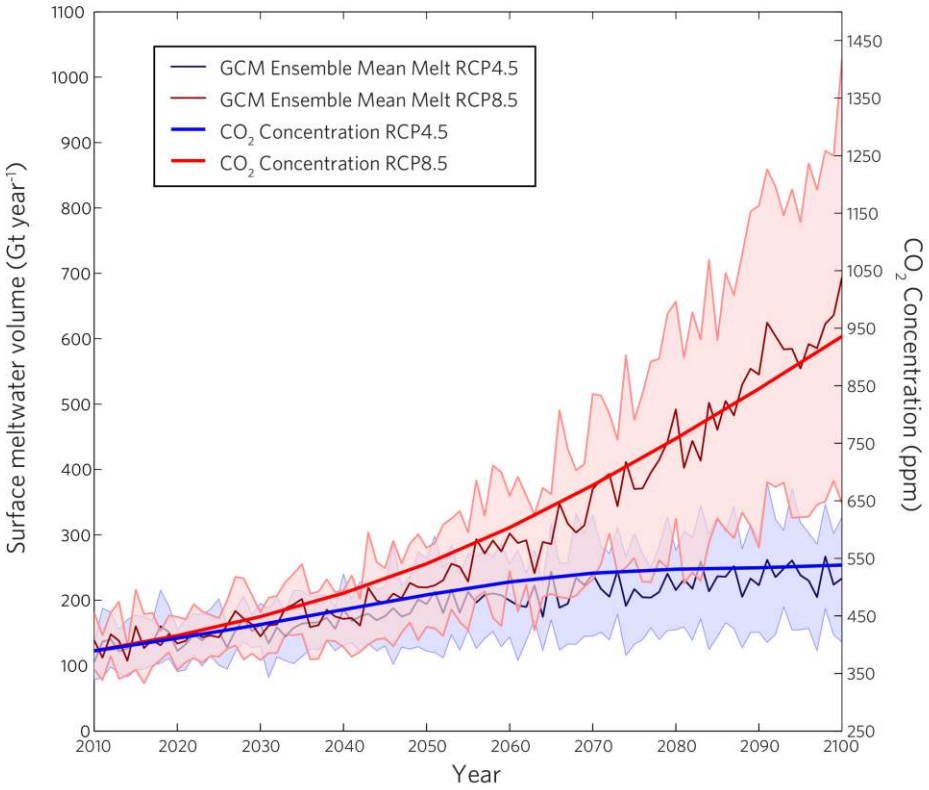

Supplementary Figure 5.
A clear connection exists between the projected Antarctic meltwater volume and atmospheric CO_2 concentrations under RCP4.5 and RCP8.5 (CO_2 time series from ref. 8). The future volume of meltwater produced at the Antarctic ice sheet surface is a function of future changes in radiative forcing, in which atmospheric CO_2 concentrations play an integral role.

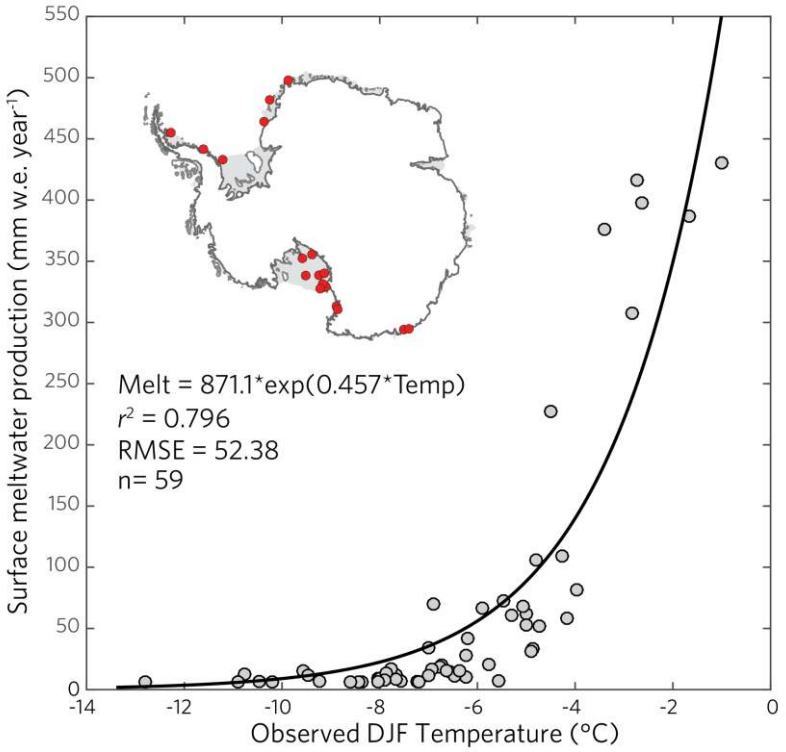

Supplementary Figure 6.
An observationally constrained melt-temperature relationship using satellite-derived surface meltwater production from QuikSCAT[9] and mean summer (DJF) air temperatures at 18 AWS and research station locations in the SCAR READER database[1] (red points on map). We examined all locations over ice with complete DJF observations during at least one year of the QuikSCAT record (1999–2000 to 2000–2009) and within a QuikSCAT grid cell detected as melting. Annual meltwater production estimated from QuikSCAT was taken from the corresponding year and grid cell containing each air temperature observation. Despite challenges inherent to this comparison including temporal mismatch between observation methods and the coarse satellite spatial resolution relative to the point scale[10], a strong nonlinear melt-temperature relationship is evident and well characterized by an exponential regression model (black line). The derived exponential relationship is strong, although data paucity at intermediate and high melt-temperature levels limit its predictive ability. This relationship is nevertheless in close agreement with our main (and independent) melt-T_{2m} sensitivity analysis that is constrained largely by coupled-climate snowpack modeling (Fig. 1a), and thereby provides additional, empirical support for melt-T_{2m} nonlinearity across Antarctica.

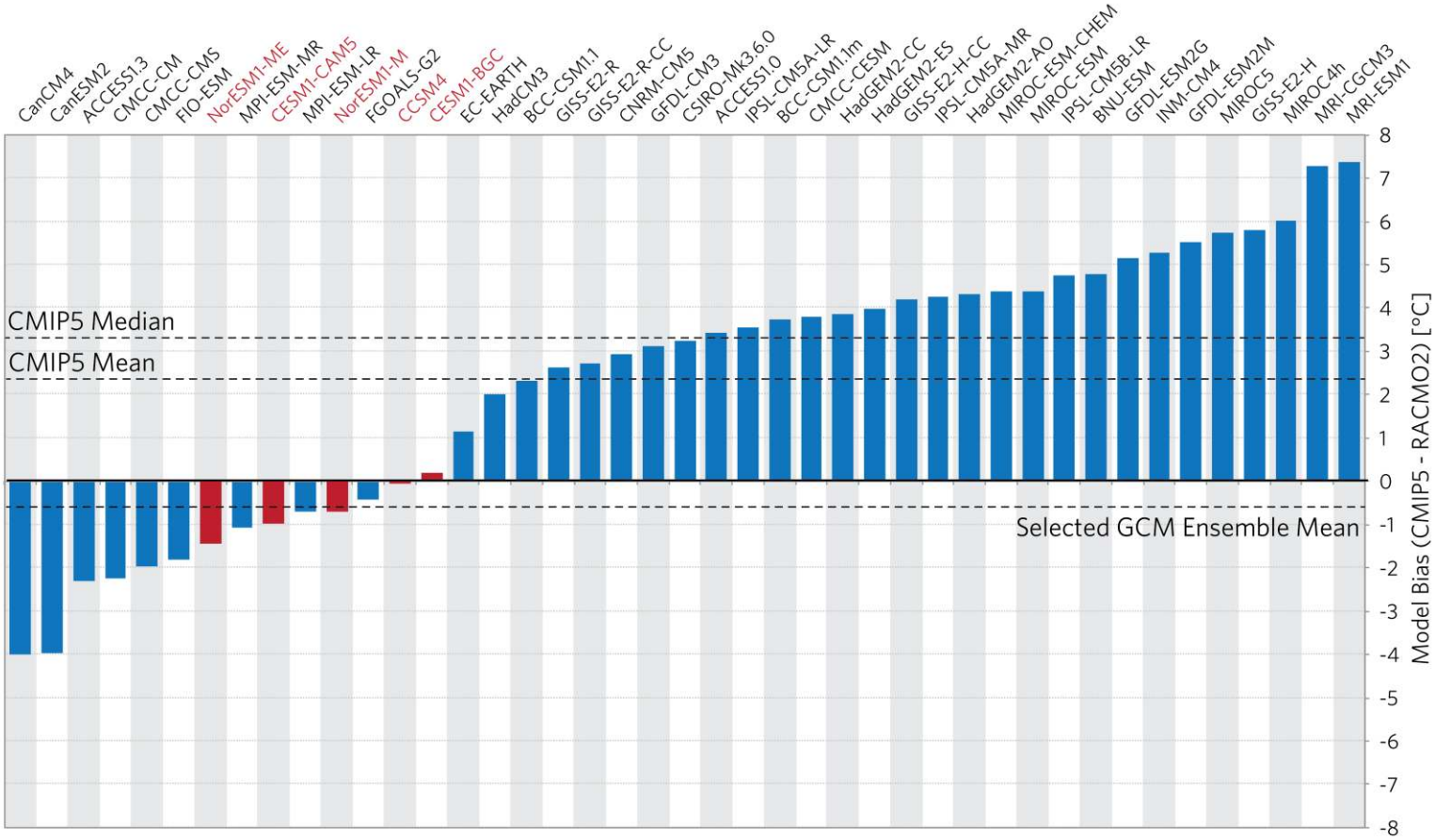

Supplementary Figure 7.
Absolute DJF-mean T_{2m} bias over all Antarctic ice shelves for 43 CMIP5-based[11] GCMs relative to ERA-Interim-forced RACMO2 at 27-km. Models selected for their Antarctic T_{2m} projections are indicated in red (see Supplementary Table 3), as are the mean DJF T_{2m} biases of these selected models and mean and median biases of the broader CMIP5 multimodel ensemble.

	Ice Shelf	**QuikSCAT** 2000-2009	**RACMO2** (27-km) ERA-Interim 1980-2009	**RACMO2** (48-km) ERA-Interim 1980-2009	**RACMO2** EC-Earth RCP4.5 2010-2099	**RACMO2** EC-Earth RCP8.5 2010-2099
AP	Bach	1 (225)	3 (6)	3 (2)	9 (2)	9 (2)
AP	George VI	1 (1186)	3 (31)	3 (9)	9 (9)	9 (9)
AP	Larsen A	No data	1 (5)	No data	No data	No data
AP	Larsen B	No data	2 (6)	2 (2)	No data	No data
AP	Larsen C	1 (2490)	3 (59)	3 (22)	9 (22)	9 (22)
AP	Larsen D	1 (1193)	3 (31)	3 (10)	9 (10)	9 (10)
AP	Scar Inlet	1 (141)	3 (3)	3 (1)	9 (1)	9 (1)
AP	Stange	1 (586)	3 (18)	3 (5)	9 (5)	9 (5)
AP	Wilkins	1 (698)	3 (17)	3 (6)	9 (6)	9 (6)
WA	Abbot	1 (1625)	3 (42)	3 (16)	9 (16)	9 (16)
WA	Cosgrove	1 (150)	3 (4)	3 (2)	9 (2)	9 (2)
WA	Crosson	1 (122)	3 (3)	3 (2)	9 (2)	9 (2)
WA	Dotson	1 (236)	3 (5)	3 (2)	9 (2)	9 (2)
WA	Getz	1 (1686)	3 (49)	3 (14)	9 (14)	9 (14)
WA	Nickerson	1 (362)	3 (7)	3 (2)	9 (2)	9 (2)
WA	Pine Island	1 (304)	3 (7)	3 (2)	9 (2)	9 (2)
WA	Ross	1 (24307)	3 (652)	3 (215)	9 (215)	9 (215)
WA	Sulzberger	1 (680)	3 (19)	3 (6)	9 (6)	9 (6)
WA	Thwaites	1 (219)	3 (6)	3 (2)	9 (2)	9 (2)
WA	Venable	1 (164)	3 (3)	3 (2)	9 (2)	9 (2)
WL	Amery	1 (2876)	3 (71)	3 (29)	9 (29)	9 (29)
WL	Conger	1 (125)	3 (3)	3 (2)	9 (2)	9 (2)
WL	Cook	1 (214)	3 (5)	3 (3)	9 (3)	9 (3)
WL	Dibble	1 (79)	3 (2)	3 (1)	9 (1)	9 (1)
WL	Holmes	1 (94)	3 (3)	3 (1)	9 (1)	9 (1)
WL	Mertz	1 (295)	3 (9)	3 (2)	9 (2)	9 (2)
WL	Moscow	1 (250)	3 (7)	3 (1)	9 (1)	9 (1)
WL	Publications	1 (87)	3 (3)	3 (1)	9 (1)	9 (1)
WL	Rennick	1 (124)	3 (2)	3 (1)	9 (1)	9 (1)
WL	Shackleton	1 (1729)	3 (41)	3 (15)	9 (15)	9 (15)
WL	Totten	1 (401)	3 (12)	3 (3)	9 (3)	9 (3)
WL	West	1 (866)	3 (21)	3 (8)	9 (8)	9 (8)
DML	Atka	1 (99)	3 (2)	3 (1)	9 (1)	9 (1)
DML	Baudouin	1 (1664)	3 (44)	3 (14)	9 (14)	9 (14)
DML	Borchgrevink	1 (876)	3 (23)	3 (9)	9 (9)	9 (9)
DML	Brunt	1 (1683)	3 (44)	3 (13)	9 (13)	9 (13)
DML	Unnamed (23°E)	1 (190)	3 (5)	3 (2)	9 (2)	9 (2)
DML	Ekstrom	1 (356)	3 (9)	3 (3)	9 (3)	9 (3)
DML	Filchner	1 (5108)	3 (135)	3 (46)	9 (46)	9 (46)
DML	Fimbul	1 (2057)	3 (56)	3 (19)	9 (19)	9 (19)
DML	Jelbart	1 (561)	3 (15)	3 (6)	9 (6)	9 (6)
DML	Lazarev	1 (434)	3 (12)	3 (4)	9 (4)	9 (4)
DML	Nivl	1 (379)	3 (12)	3 (5)	9 (5)	9 (5)
DML	Prince Harald	1 (269)	3 (7)	3 (3)	9 (3)	9 (3)

DML	Quar	1 (112)	3 (2)	3 (1)	9 (1)	9 (1)
DML	Riiser-Larsen	1 (2293)	3 (63)	3 (26)	9 (26)	9 (26)
DML	Ronne	1 (16445)	3 (435)	3 (145)	9 (145)	9 (145)
DML	Vigrid	1 (118)	3 (2)	3 (1)	9 (1)	9 (1)

Supplementary Table 1.
Listing of observed and modeled data used to establish the melt-T_{2m} sensitivity and calibration curve show in Fig. 1a. Values of each cell indicate the number of data points (i.e., decadal periods) from each method for particular ice shelves and floating outlet glacier termini in Fig 1a. Values in parentheses indicate number of discrete grid cells available in each method for each ice shelf after masking with an updated version of the MODIS outline of Antarctica[12]. For the melt-T_{2m} calibration (Fig. 1a), T_{2m} data coinciding with QuikSCAT melt observations[9] were taken from RACMO2 forced by ERA-Interim at 27-km grid resolution. All melt and T_{2m} data were averaged spatially across ice shelf grid cells and decadally beginning in 2000–2009 for consistency between reanalysis-forced RACMO2 simulations and QuikSCAT observations. An exception exists for Larsen A and B (in Fig. 1a, Fig. 1b, and Supplementary Fig. 2), for which data were averaged over available decades ending in the years associated with their collapses (i.e., 1986–1995 for Larsen A, 1993–2002 for Larsen B). Ice shelves are organized in this table by region indicated in first column and shown in Fig. 4b (AP: Antarctic Peninsula; WA: West Antarctica; WL: Wilkes Land; DML: Dronning Maud Land). Note that after spatial downscaling and bias correction, the number of grid cells used in future projections from the GCM Ensemble (i.e., Figs. 3b, 4a) are identical to that as RACMO2 at 48-km.

	RACMO2-ERA-Interim 27-km	**RACMO2-ERA-Interim 48-km**	**RACMO2-EC-Earth (Historical)**	**RACMO2-HadGEM2-ES (Historical)**
Mean Antarctic meltwater volume (1980–2005) (Gt $year^{-1}$)	105.59	83.43	112.43	199.09
Bias (w.r.t. RACMO2-ERA-Interim 27-km) (Gt $year^{-1}$)	-	-22.16	6.84	93.51
Bias (w.r.t. RACMO2-ERA-Interim 48-km) (Gt $year^{-1}$)	22.16	-	29.00	115.67

Supplementary Table 2.
Biases in the Antarctic-wide meltwater volume simulated between RACMO2 forced by ERA-Interim at two grid resolutions and two GCMs under their CMIP5 Historical experiments. RACMO2 forced by EC-Earth produces very similar results to the ERA-Interim forcings, whereas RACMO2 forced by HadGEM2-ES shows large positive melt biases.

Model	Spatial Resolution	Driving Dataset	Timespans utilized (CMIP5 Experiment)	Ensemble members
RACMO2	27-km	ERA-Interim Reanalysis (ref. 13)	1980-2010	1
RACMO2	48-km	ERA-Interim Reanalysis (ref. 13)	1980-2012	1
RACMO2	48-km	EC-Earth2.3 (r1i1p1) (ref. 14)	2007-2100 (RCP4.5, RCP8.5)	1 (all experiments)
CCSM4 (ref. 15)	1.25° longitude, 0.94° latitude	N/A	1851-2005 (historicalNat) 1980-2005 (Historical) 2007-2100 (RCP4.5, RCP8.5)	4 (historicalNat) 6 (Historical, RCP4.5, RCP8.5)
CESM1(BGC) (ref. 16)	1.25° longitude, 0.94° latitude	N/A	1980-2005 (Historical) 2007-2100 (RCP4.5, RCP8.5)	1 (all experiments)
CESM1(CAM5) (ref. 17)	1.25° longitude, 0.94° latitude	N/A	1851-2005 (historicalNat) 1980-2005 (Historical) 2007-2100 (RCP4.5, RCP8.5)	3 (all experiments)
NorESM1-M (ref. 18)	2.5° longitude, 1.895° latitude	N/A	1851-2005 (historicalNat) 1980-2005 (Historical) 2007-2100 (RCP4.5, RCP8.5)	3 (Historical) 1 (historicalNat, RCP4.5, RCP8.5)
NorESM1-ME (ref. 18)	2.5° longitude, 1.895° latitude	N/A	1980-2005 (Historical) 2007-2100 (RCP4.5, RCP8.5)	1 (all experiments)

Supplementary Table 3.
Regional and global climate model configurations used in this study. Where multiple ensemble members were available, the ensemble mean was calculated. Whereas Historical experiments (i.e., including all transient forcing agents) were available from the five GCMs, historicalNat (i.e., including only natural forcing agents) were only available from three.

Supplementary References

1. Turner, J. *et al.* The SCAR READER Project: Toward a High-Quality Database of Mean Antarctic Meteorological Observations. *J. Climate* **17,** 2890–2898 (2004).
2. Vaughan, D. G. & Doake, C. S. M. Recent atmospheric warming and retreat of ice shelves on the Antarctic Peninsula. *Nature* **379,** 328–331 (1996).
3. Scambos, T. A., Hulbe, C., Fahnestock, M. & Bohlander, J. The link between climate warming and break-up of ice shelves in the Antarctic Peninsula. *J. Glaciol.* **46,** 516–530 (2000).
4. Scambos, T., Hulbe, C. & Fahnestock, M. in *Antarctic Research Series* (eds. Domack, E. et al.) **79,** 79–92 (American Geophysical Union, 2003).
5. Scambos, T. *et al.* Ice shelf disintegration by plate bending and hydro-fracture: Satellite observations and model results of the 2008 Wilkins ice shelf break-ups. *Earth Planet. Sc. Lett.* **280,** 51–60 (2009).
6. Braun, M. & Humbert, A. Recent Retreat of Wilkins Ice Shelf Reveals New Insights in Ice Shelf Breakup Mechanisms. *IEEE Geosci. Remote S.* **6,** 263–267 (2009).
7. Braun, M., Humbert, A. & Moll, A. Changes of Wilkins Ice Shelf over the past 15 years and inferences on its stability. *Cryosphere* **3,** 41–56 (2009).
8. Van Vuuren, D. P. *et al.* The representative concentration pathways: an overview. *Climatic Change* **109,** 5–31 (2011).
9. Trusel, L. D., Frey, K. E., Das, S. B., Kuipers Munneke, P. & van den Broeke, M. R. Satellite-based estimates of Antarctic surface meltwater fluxes. *Geophys. Res. Lett.* **40,** 6148–6153 (2013).
10. Trusel, L. D., Frey, K. E. & Das, S. B. Antarctic surface melting dynamics: Enhanced perspectives from radar scatterometer data. *J. Geophys. Res.* **117,** F02023 (2012).
11. Taylor, K. E., Stouffer, R. J. & Meehl, G. A. An Overview of CMIP5 and the Experiment Design. *Bull. Amer. Meteorol. Soc.* **93,** 485–498 (2012).
12. Haran, T., Bohlander, J., Scambos, T., Painter, T. & Fahnestock, M. *MODIS Mosaic of Antarctica (MOA) Image Map* (National Snow and Ice Data Center, Boulder, 2005).
13. Dee, D. P. *et al.* The ERA-Interim reanalysis: configuration and performance of the data assimilation system. *Q. J. R. Meteorol. Soc.* **137,** 553–597 (2011).
14. Hazeleger, W. *et al.* EC-Earth V2.2: description and validation of a new seamless earth system prediction model. *Clim. Dyn.* **39,** 2611–2629 (2012).
15. Gent, P. R. *et al.* The Community Climate System Model Version 4. *J. Climate* **24,** 4973–4991 (2011).
16. Long, M. C., Lindsay, K., Peacock, S., Moore, J. K. & Doney, S. C. Twentieth-Century Oceanic Carbon Uptake and Storage in CESM1(BGC)*. *J. Climate* **26,** 6775–6800 (2013).
17. Meehl, G. A. *et al.* Climate Change Projections in CESM1(CAM5) Compared to CCSM4. *J. Climate* **26,** 6287–6308 (2013).
18. Bentsen, M. *et al.* The Norwegian Earth System Model, NorESM1-M – Part 1: Description and basic evaluation of the physical climate. *Geosci. Model Dev.* **6,** 687–720 (2013).